Symmetry Guide to Ferroaxial Transitions

J. Hlinka,* J. Privratska, P. Ondrejkovic, and V. Janovec
Institute of Physics, The Czech Academy of Sciences, Na Slovance 2, 182 21 Prague 8, Czech Republic
(Received 17 February 2016; published 28 April 2016)

The 212 species of the structural phase transitions with a macroscopic symmetry breaking are inspected with respect to the occurrence of the ferroaxial order parameter, the electric toroidal moment. In total, 124 ferroaxial species are found, some of them being also fully ferroelectric (62) or fully ferroelastic ones (61). This ensures a possibility of electrical or mechanical switching of ferroaxial domains. Moreover, there are 12 ferroaxial species that are neither ferroelectric nor ferroelastic. For each species, we have also explicitly worked out a canonical form for a set of representative equilibrium property tensors of polar and axial nature in both high-symmetry and low-symmetry phases. This information was gathered into the set of 212 mutually different symbolic matrices, expressing graphically the presence of nonzero independent tensorial components and the symmetry-imposed links between them, for both phases simultaneously. Symmetry analysis reveals the ferroaxiality in several currently debated materials, such as VO_2, $LuFe_2O_4$, and URu_2Si_2.

DOI: 10.1103/PhysRevLett.116.177602

Recently, crystalline substances of a new type, so-called ferroaxial crystals, have been brought to the fore [1–4]. A canonical example of the ferroaxial [2] material is the $CaMn_7O_{12}$ crystal. Ferroaxiality can be considered an analogue to ferroelectricity. Both phenomena refer to a material in which a structural symmetry-breaking phase transition is associated with a macroscopic order parameter of vectorial nature. The order parameter in a ferroelectric material is a polar vector, electric polarization **P**, while, in the case of a ferroaxial crystal, the order parameter is a macroscopic structural distortion with an axial vector symmetry. It can be represented by an electric toroidal moment **A** [5–7], which is a time-reversal-invariant analogue of the magnetic toroidal moment **T** [5,7,8].

There is, however, one very important difference between the ferroelectric and ferroaxial materials. The electric polarization **P** is a conjugated variable to the electric field, so the ferroelectric domains can be directly addressed by macroscopic electric fields. On the other hand, there are no readily available sources of a "macroscopic ferroaxial field" conjugated to **A**.

Therefore, it is essential to identify whether and under which conditions the electric toroidal moment can be switched electrically or mechanically. Here we derive, solely on symmetry grounds, a list of all possible symmetry reductions that would lead to materials in which the ferroaxial domains could be addressed by a stress and electric fields, respectively.

Species.—It is well known that each periodic crystal belongs to one of the six crystal families and that its nonmagnetic macroscopic symmetry is described by one of the 32 crystallographic point groups (see Table I). Among them, there are 13 pyroaxial groups which allow for the electric toroidal moment (subgroups of the ∞/m group [7,9]). Ferroaxiality is associated with the *new* components of **A**, resulting from a symmetry-breaking phase transition. An analysis of symmetry-breaking phase transitions requires us to consider simultaneously the symmetry operations of the high- and low-symmetry phases as well as the exact correspondence between them. Distinct types of symmetry reductions are called species [10–18] It is known that symmetry reductions of 32 crystallographic point groups can be classified among 212 "nonmagnetic" Aizu species [15,16,19–21].

The 212 species can be subdivided into six categories, depending on the crystal family of the parent (high-symmetry) phase point group, and are labeled accordingly. There are 1 triclinic, 6 monoclinic, 12 orthorhombic, 46 tetragonal, 80 hexagonal, and 67 cubic species. The triclinic, monoclinic, and orthorhombic species can be uniquely identified by the symbol $G > F$, where G and F are standard crystal class symbols of the high- and low-symmetry phases. Any of these species corresponds to a group-subgroup pair connected in Fig. 1 by a top-down path having the top (G) vertex in a bold rectangle frame. For example, $mmm > 2$ stands for one of the orthorhombic species.

Some tetragonal, hexagonal, and cubic G classes contain nonequivalent mirror planes or twofold axes. To indicate

TABLE I. List of 32 crystal classes. The symbols of *pyroaxial* classes are followed by a † superscript.

Crystal family	Crystal classes
Triclinic	$1^\dagger$, $\bar{1}^\dagger$
Monoclinic	$2^\dagger$, $m^\dagger$, $2/m^\dagger$
Orthorhombic	222, $mm2$, mmm
Tetragonal	$4^\dagger$, $\bar{4}^\dagger$, $4/m^\dagger$, 422, $4mm$, $\bar{4}2m$, $4/mmm$
Hexagonal	$3^\dagger$, $\bar{3}^\dagger$, 32, $3m$, $\bar{3}m$, $6^\dagger$, $\bar{6}^\dagger$, $6/m^\dagger$, 622, $6mm$, $\bar{6}m2$, $6/mmm$
Cubic	23, $m\bar{3}$, 432, $\bar{4}3m$, $m\bar{3}m$

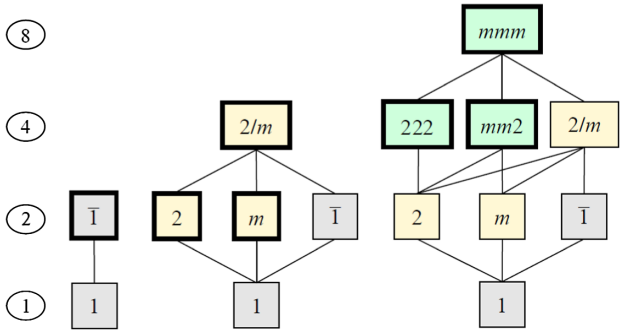

FIG. 1. Triclinic (left panel), monoclinic (middle panel), and orthorhombic (right panel) species. Each vertex pair connected by a top-down path starting in a bold-frame rectangle corresponds to one species. Note that a species is identified by the top and bottom groups so that several paths may give the same species. Numbers in ovals give the order of the point group.

which of these nonequivalent mirrors or twofold axes is preserved in F, the crystal class label of F is optionally decorated with additional subscripts, specifying the orientation of the preserved symmetry elements with respect to those of the parent group G. Thus, $2_|$ and 2_- in F's of tetragonal and hexagonal species stand for twofold axes parallel and perpendicular to the unique axis of G, while $m_|$ and m_- stand for the mirror plane with its normal parallel and perpendicular to this axis, respectively (see the left inset in Fig. 2). Similarly, 2_+, $2_\backslash$, m_+, and $m_\backslash$ in F's of the cubic species stand for twofold axes and mirrors with $\langle 100\rangle$, $\langle 110\rangle$, $\{100\}$, and $\{110\}$ orientations with respect to the cubic axes, respectively. The decorated symbols of the "oriented" subgroups F facilitate a compact presentation of all species in the form of family graphs (see Fig. 2) or in the form of a list (see Fig. 3).

Orientational domains.—In general, the low-symmetry phase of any macroscopic symmetry-breaking phase transition exists in two or more macroscopically distinct, but energetically equivalent, "orientational" states [11,22,23]. These states may coexist in the crystal as macroscopic domains. When some or all domain states differ in components of the spontaneous polarization, the transition is called partial or full ferroelectric, respectively. This attribute is common to all transitions within a species [11,22]. It can be derived for other spontaneous tensors as well. Using the method outlined in Ref. [17,18], we have determined the number of the distinct ferroaxial domain states in all 212 species. The occurrence of the ferroaxiality in each species is displayed together with its ferroelectric and ferroelastic character in Fig. 3.

Switching by the electric field or stress.—The listing in Fig. 3 immediately shows that there are 124 different ferroaxial species in total. Out of them, 62 species are also

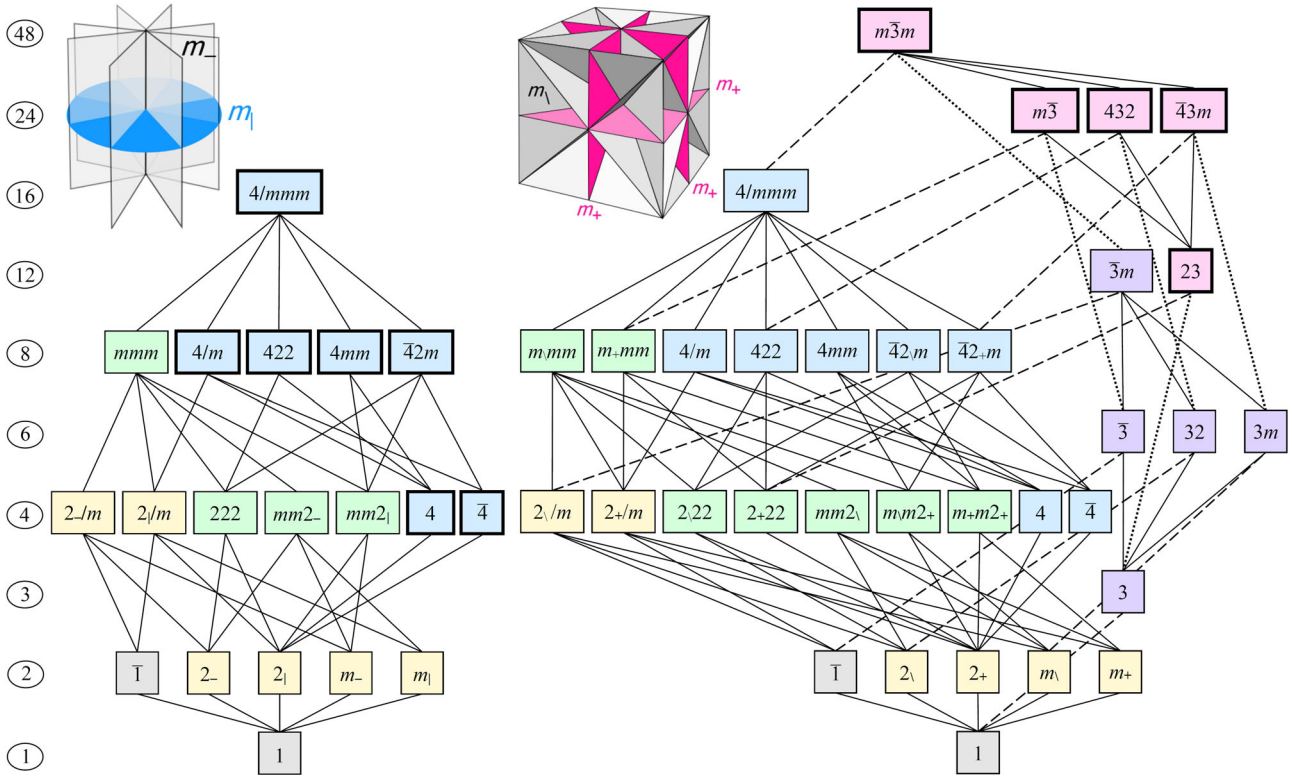

FIG. 2. Subordination of tetragonal and cubic species. Each top-down connected path starting in one of the bold-frame vertices corresponds to one of the tetragonal (left panel) or cubic (right panel) species. Note that several paths may give the same species. The insets clarify the meaning of the $m_|$, m_-, $m_\backslash$, and m_+ symbols introduced in the text. Full, dashed, and dotted lines indicate group-subgroup relations of index 2, 3, and 4, respectively. Numbers in ovals give the order of the point group.

fully ferroelectric ones. These species describe the cases where any desired ferroaxial state could be selected by an electric field. Likewise, the full ferroelastic ferroaxial species correspond to phases in which the electric toroidal moment **A** can be switched mechanically. This is the case of the "ferroaxial" [2] phase transition in $CaMn_7O_{12}$ at 440 K. Therefore, a recently reported ferroelastic domain switching in this material [4] induced by uniaxial stress actually represents a clean example of a mechanically achieved ferroaxial domain switching.

No.	G	F	n	a	b	c
1	$\bar{1}$	1	2	●	○	○
2	2	1	2	●	●	●
3	m	1	2	●	●	●
4	$2/m$	m	2	●	○	○
5	$2/m$	2	2	●	○	○
6	$2/m$	$\bar{1}$	2	○	●	●
7	$2/m$	1	4	●	◐	◐
8	222	2	2	●	●	●
9	222	1	4	●	●	●
10	$mm2$	m	2	●	●	●
11	$mm2$	2	2	○	●	●
12	$mm2$	1	4	●	●	●
13	mmm	$mm2$	2	●	○	○
14	mmm	222	2	○	○	○
15	mmm	$2/m$	2	○	●	●
16	mmm	m	4	●	◐	◐
17	mmm	2	4	◐	◐	◐
18	mmm	$\bar{1}$	4	○	●	●
19	mmm	1	8	●	◐	◐
20	4	$2_\vert$	2	○	●	○
21	4	1	4	●	●	●
22	$\bar{4}$	$2_\vert$	2	●	●	○
23	$\bar{4}$	1	4	●	●	●
24	$4/m$	$\bar{4}$	2	○	○	○
25	$4/m$	4	2	●	○	○
26	$4/m$	$2_\vert/m$	2	○	●	○
27	$4/m$	$m_\vert$	4	●	◐	○
28	$4/m$	$2_\vert$	4	◐	◐	○
29	$4/m$	$\bar{1}$	4	○	●	●
30	$4/m$	1	8	●	◐	◐
31	422	4	2	●	○	●
32	422	222	2	○	●	○
33	422	$2_\vert$	4	◐	◐	◐
34	422	2_-	4	●	◐	●
35	422	1	8	●	●	●
36	$4mm$	4	2	○	○	●
37	$4mm$	$mm2_\vert$	2	○	●	○
38	$4mm$	m_-	4	●	●	●
39	$4mm$	$2_\vert$	4	○	◐	◐
40	$4mm$	1	8	●	●	●
41	$\bar{4}2m$	$\bar{4}$	2	○	○	●
42	$\bar{4}2m$	$mm2_\vert$	2	●	●	○
43	$\bar{4}2m$	222	2	○	●	○
44	$\bar{4}2m$	m_-	4	●	●	●
45	$\bar{4}2m$	$2_\vert$	4	◐	◐	◐
46	$\bar{4}2m$	2_-	4	●	●	●
47	$\bar{4}2m$	1	8	●	●	●
48	$4/mmm$	$\bar{4}2m$	2	○	○	○
49	$4/mmm$	$4mm$	2	●	○	○
50	$4/mmm$	422	2	○	○	○
51	$4/mmm$	$4/m$	2	○	○	●
52	$4/mmm$	$\bar{4}$	4	○	○	◐
53	$4/mmm$	4	4	◐	○	◐
54	$4/mmm$	mmm	2	○	●	○
55	$4/mmm$	$mm2_\vert$	4	◐	◐	○
56	$4/mmm$	$mm2_-$	4	●	◐	○
57	$4/mmm$	222	4	○	◐	○
58	$4/mmm$	$2_\vert/m$	4	○	●	◐
59	$4/mmm$	$2_-/m$	4	○	●	●
60	$4/mmm$	$m_\vert$	8	●	◐	◐
61	$4/mmm$	m_-	8	●	◐	◐
62	$4/mmm$	$2_\vert$	8	◐	◐	◐
63	$4/mmm$	2_-	8	◐	◐	◐
64	$4/mmm$	$\bar{1}$	8	○	●	●
65	$4/mmm$	1	16	●	◐	◐
66	3	1	3	●	●	●
67	$\bar{3}$	3	2	●	○	○
68	$\bar{3}$	$\bar{1}$	3	○	●	●
69	$\bar{3}$	1	6	●	◐	◐
70	32	3	2	●	○	●
71	32	2_-	3	●	●	●
72	32	1	6	●	●	●
73	$3m$	3	2	○	○	●
74	$3m$	m_-	3	●	●	●
75	$3m$	1	6	●	●	●
76	$\bar{3}m$	$3m$	2	●	○	○
77	$\bar{3}m$	32	2	○	○	○
78	$\bar{3}m$	$\bar{3}$	2	○	○	●
79	$\bar{3}m$	3	4	◐	○	◐
80	$\bar{3}m$	$2_-/m$	3	○	●	●
81	$\bar{3}m$	m_-	6	●	◐	◐
82	$\bar{3}m$	2_-	6	●	◐	◐
83	$\bar{3}m$	$\bar{1}$	6	○	●	●
84	$\bar{3}m$	1	12	●	◐	◐
85	6	3	2	○	○	○
86	6	$2_\vert$	3	○	●	○
87	6	1	6	●	●	●
88	$\bar{6}$	3	2	●	○	○
89	$\bar{6}$	$m_\vert$	3	●	●	○
90	$\bar{6}$	1	6	●	●	●
91	$6/m$	$\bar{6}$	2	○	○	○
92	$6/m$	6	2	●	○	○
93	$6/m$	$\bar{3}$	2	○	○	○
94	$6/m$	3	4	◐	○	○
95	$6/m$	$2_\vert/m$	3	○	●	○
96	$6/m$	$m_\vert$	6	●	◐	○
97	$6/m$	$2_\vert$	6	◐	◐	○
98	$6/m$	$\bar{1}$	6	○	●	●
99	$6/m$	1	12	●	◐	◐
100	622	6	2	●	○	●
101	622	32	2	○	○	○
102	622	3	4	◐	○	◐
103	622	222	3	○	●	○
104	622	$2_\vert$	6	◐	●	◐
105	622	2_-	6	●	●	●
106	622	1	12	●	●	●
107	$6mm$	6	2	○	○	●
108	$6mm$	$3m$	2	○	○	○
109	$6mm$	3	4	○	○	◐
110	$6mm$	$mm2_\vert$	3	○	●	○
111	$6mm$	m_-	6	●	●	●
112	$6mm$	$2_\vert$	6	○	●	◐
113	$6mm$	1	12	●	●	●
114	$\bar{6}m2$	$\bar{6}$	2	○	○	●
115	$\bar{6}m2$	$3m$	2	●	○	○
116	$\bar{6}m2$	32	2	○	○	○
117	$\bar{6}m2$	3	4	◐	○	◐
118	$\bar{6}m2$	$mm2_-$	3	●	●	○
119	$\bar{6}m2$	$m_\vert$	6	●	●	◐
120	$\bar{6}m2$	m_-	6	●	●	●
121	$\bar{6}m2$	2_-	6	◐	●	●
122	$\bar{6}m2$	1	12	●	●	●
123	$6/mmm$	$\bar{6}m2$	2	○	○	○
124	$6/mmm$	$6mm$	2	●	○	○
125	$6/mmm$	622	2	○	○	○
126	$6/mmm$	$6/m$	2	○	○	●
127	$6/mmm$	$\bar{6}$	4	○	○	◐
128	$6/mmm$	6	4	◐	○	◐
129	$6/mmm$	$\bar{3}m$	2	○	○	○
130	$6/mmm$	$3m$	4	◐	○	○
131	$6/mmm$	32	4	○	○	○
132	$6/mmm$	$\bar{3}$	4	○	○	◐
133	$6/mmm$	3	8	◐	○	◐
134	$6/mmm$	mmm	3	○	●	○
135	$6/mmm$	$mm2_\vert$	6	◐	◐	○
136	$6/mmm$	$mm2_-$	6	●	◐	○
137	$6/mmm$	222	6	○	◐	○
138	$6/mmm$	$2_\vert/m$	6	○	●	◐
139	$6/mmm$	$2_-/m$	6	○	●	●
140	$6/mmm$	$m_\vert$	12	●	◐	◐
141	$6/mmm$	m_-	12	●	◐	◐
142	$6/mmm$	$2_\vert$	12	◐	◐	◐
143	$6/mmm$	2_-	12	◐	◐	◐
144	$6/mmm$	$\bar{1}$	12	○	●	●
145	$6/mmm$	1	24	●	◐	◐
146	23	3	4	●	●	●
147	23	2_+22	3	○	●	○
148	23	2_+	6	●	●	●
149	23	1	12	●	●	●
150	$m\bar{3}$	23	2	○	○	○
151	$m\bar{3}$	$\bar{3}$	4	○	●	●
152	$m\bar{3}$	3	8	●	◐	◐
153	$m\bar{3}$	m_+mm	3	○	●	○
154	$m\bar{3}$	m_+m2_+	6	●	◐	○
155	$m\bar{3}$	2_+22	6	○	◐	○
156	$m\bar{3}$	$2_+/m$	6	○	●	●
157	$m\bar{3}$	m_+	12	●	◐	◐
158	$m\bar{3}$	2_+	12	◐	◐	◐
159	$m\bar{3}$	$\bar{1}$	12	○	●	●
160	$m\bar{3}$	1	24	●	◐	◐
161	432	23	2	○	○	○
162	432	32	4	○	●	○
163	432	3	8	●	◐	●
164	432	422	3	○	●	○
165	432	4	6	●	◐	●
166	432	2_+22	6	○	●	○
167	432	$2_\backslash 22$	6	○	●	○
168	432	2_+	12	◐	◐	◐
169	432	$2_\backslash$	12	●	●	●
170	432	1	24	●	●	●
171	$\bar{4}3m$	23	2	○	○	○
172	$\bar{4}3m$	$3m$	4	●	●	○
173	$\bar{4}3m$	3	8	◐	◐	●
174	$\bar{4}3m$	$\bar{4}2_+m$	3	○	●	○
175	$\bar{4}3m$	$\bar{4}$	6	○	◐	●
176	$\bar{4}3m$	$m_\backslash m2_+$	6	●	●	○
177	$\bar{4}3m$	2_+22	6	○	●	○
178	$\bar{4}3m$	$m_\backslash$	12	●	●	●
179	$\bar{4}3m$	2_+	12	◐	◐	◐
180	$\bar{4}3m$	1	24	●	●	●
181	$m\bar{3}m$	$\bar{4}3m$	2	○	○	○
182	$m\bar{3}m$	432	2	○	○	○
183	$m\bar{3}m$	$m\bar{3}$	2	○	○	○
184	$m\bar{3}m$	23	4	○	○	○
185	$m\bar{3}m$	$\bar{3}m$	4	○	●	○
186	$m\bar{3}m$	$3m$	8	●	◐	○
187	$m\bar{3}m$	32	8	○	◐	○
188	$m\bar{3}m$	$\bar{3}$	8	○	◐	●
189	$m\bar{3}m$	3	16	◐	◐	◐
190	$m\bar{3}m$	$4/mmm$	3	○	●	○
191	$m\bar{3}m$	$\bar{4}2_+m$	6	○	◐	○
192	$m\bar{3}m$	$\bar{4}2_\backslash m$	6	○	◐	○
193	$m\bar{3}m$	$4mm$	6	●	◐	○
194	$m\bar{3}m$	422	6	○	◐	○
195	$m\bar{3}m$	$4/m$	6	○	◐	●
196	$m\bar{3}m$	$\bar{4}$	12	○	◐	◐
197	$m\bar{3}m$	4	12	◐	◐	◐
198	$m\bar{3}m$	m_+mm	6	○	●	○
199	$m\bar{3}m$	$m_\backslash mm$	6	○	●	○
200	$m\bar{3}m$	m_+m2_+	12	◐	◐	○
201	$m\bar{3}m$	$m_\backslash m2_+$	12	◐	◐	○
202	$m\bar{3}m$	$mm2_\backslash$	12	●	◐	○
203	$m\bar{3}m$	2_+22	12	○	◐	○
204	$m\bar{3}m$	$2_\backslash 22$	12	○	◐	○
205	$m\bar{3}m$	$2_+/m$	12	○	●	◐
206	$m\bar{3}m$	$2_\backslash/m$	12	○	●	●
207	$m\bar{3}m$	m_+	24	●	◐	◐
208	$m\bar{3}m$	$m_\backslash$	24	●	◐	◐
209	$m\bar{3}m$	2_+	24	◐	◐	◐
210	$m\bar{3}m$	$2_\backslash$	24	◐	◐	◐
211	$m\bar{3}m$	$\bar{1}$	24	○	●	●
212	$m\bar{3}m$	1	48	●	◐	◐

FIG. 3. List of 212 nonmagnetic species $G > F$. "No.," G, and F stand for the serial number of species and the symmetry class of the high-symmetry and low-symmetry phases. A total number of the orientational domain states appears in column n. Full, semiopen, and open circles in column a stand for full ferroelectric, partial ferroelectric, and nonferroelectric transitions. Corresponding symbols in column b and c refer to ferroelasticity and ferroaxiality.

Other material property tensors.—The given species allows us to infer systematic changes in many other tensorial properties. Nye has conveniently listed the symmetry-allowed form of several basic material property tensors—the tensors of linear elasticity, piezoelectricity, thermal expansion, dielectric susceptibility, and pyroelectricity for each of the 32 crystal classes in a corresponding 10×10 symbolic matrix (array) [24]. Here, we extend these matrices to a 13×13 format by including also the *axial tensors* up to the third rank. The layout of such matrices is shown in Fig. 4(a). Interestingly, each crystal class has a distinct 13×13 matrix. This is not true for the 10×10 Nye's matrices (for example, the 10×10 matrices of the 23 and $\bar{4}3m$ classes are identical).

In order to reveal the symmetry constraints released at the transition of a given species $G > F$, the tensors of both G and F have to be inspected simultaneously. This can be achieved in three steps by (i) selecting a representative domain state of F, (ii) expressing material tensors of both phases in the common rectangular (Cartesian) coordinate system, attached in the standard way to the symmetry elements of G, and (iii) displaying both results in a single matrix, indicating the nonzero components and constraints present in both phases in black, and the additional nonzero components and changes appearing due to the symmetry decrease in red.

This procedure has previously been applied to various tensor properties [20,27,28]. However, the combination of polar and axial tensors as worked out here is of singular interest: we have calculated such "dichromatic" matrices for all 212 species and realized that all of them are distinct.

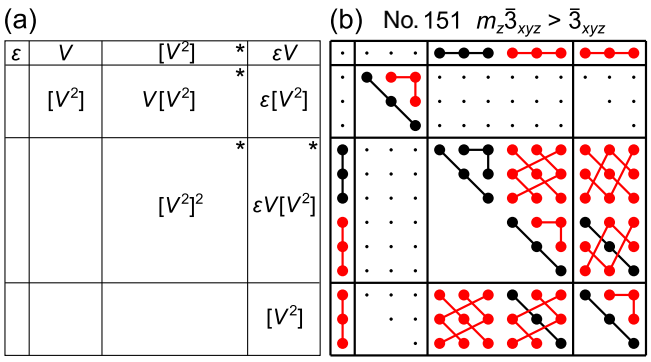

FIG. 4. Form of the canonical property tensors. (a) Layout of the extended Nye's matrix. Original entries of the Nye's matrix [24], labeled by Jahn's symbols [25] V, $[V^2]$, $V[V^2]$, and $[V^2]^2$, stand for polar tensors with the internal symmetry of the pyroelectricity, permittivity, piezoelectricity, and elastic tensors, respectively. Added entries, labeled by Jahn's symbols ε, εV, $\varepsilon[V^2]$, and $\varepsilon V[V^2]$, stand for axial tensors with the symmetry of pseudoscalar, pyroaxiality, optical activity (symmetric gyration), and electrogyration tensor, respectively. Tensors marked with a $\star$ are contracted as in Refs. [24,26]. (b) Example of dichromatic matrix for species No. 151. Red (black) symbols refer to the components nonzero in the low-symmetry phase (in both phases). Lines are connecting equal components.

Thus, by inspection of the symmetry constraints in the tensors listed in Fig. 4(a), i.e., by checking changes in a few selected *macroscopic* properties, the species can be uniquely determined. An example of the dichromatic matrix with new components of electrogyration tensor ($\varepsilon V[V^2]$) corresponding to various feroaxial spontaneous properties at a ferroaxial transition. For the sake of convenience, the dichromatic matrices of all species are also listed in the Supplemental Material [26] as well as in the interactive online tool [29].

Pure ferroaxial species.—It is worth emphasizing that some ferroaxial transitions are neither ferroelectric nor ferroelastic. In order to achieve reversible switching of the ferroaxial domain states in such "pure" ferroaxial materials, the sole application of the electric field or the sole anisotropic stress will not be sufficient. In spite of this, the ferroaxial order parameter could possibly be influenced by a nonlinear coupling to an electric field and stress. Another alternative is perhaps to exploit the short-range interaction across an epitaxial interface between the pure ferroaxial material and a convenient auxiliary, electrically switchable ferroelectric ferroaxial material (similar to the way the exchange bias is sometimes used to switch antiferromagnetic materials grown on suitable ferromagnets).

In total, there are 12 pure ferroaxial species [30]. Among them, 36, 73, and 107 are associated with an onset of the enantiomorphism and the symmetric gyration tensor of the optical activity ($\varepsilon[V^2]$) is induced in five of them [31]. The onset of the piezoelectric tensor ($V[V^2]$) components in the eight pure-ferroaxial ferroelastoelectric [17,18,32,33] species allows us to address the **A** domains by simultaneously applied electric and elastic fields. Interestingly, only four pure-ferroaxial species are partial ones (No. 52, 109, 127, and 132). In these cases, the symmetry reduction involves an intermediate point group, in a similar way as in the hybrid improper ferroelectric phase transitions [34–36].

Identified ferroaxial materials.—A particular case of the macroscopic symmetry reduction can be easily located in Fig. 3 because the species are first arranged according to the increasing symmetry of G and then according to the decreasing symmetry of F. This can be used to search for the ferroaxiality in materials with the known symmetry reduction. Interestingly, the very first known ferroelectric material, Rochelle salt [37–39], actually belongs to a fully ferroaxial species (No. 8). Other materials exhibit ferroaxiality, e.g., the ferroelectric phase of hexagonal barium titanate [40] below 74 K (No. 142), the "proper ferroelastic" phase of lithium ammonium tatrate [41] (No. 8), the polar but nonferroelectric ferroelastic phase of lithium ammonium sulphate [42] (No. 11), the charge-ordered phase of the "electronic ferroelectric" crystal [43–45] $LuFe_2O_4$ (No. 81) and the metal-insulator phase transition in vanadium dioxide [46,47] (No. 58). Finally, there is also an example of a pure and full ferroaxial phase, realized in the charge density wave transition of a heavy-fermion system [48,49] URu_2Si_2

(No. 51). Thus, the macroscopic order parameter of its "hidden order" phase below 17.5 K transforms as an axial vector.

Summary.—This Letter aimed to clarify which of the structural phase transitions with a macroscopic symmetry breaking are ferroaxial transitions. The list of 212 species with the associated symmetry analysis given in Fig. 3 can be used to identify ferroaxiality in the known or new materials as well as to check on whether their ferroaxial domain states can be selected by a homogeneous electric field or stress. The 13×13 dichromatic matrices of Fig. 4 can be employed as a unique species fingerprint. These matrices can be also used for the inspection of the spontaneous components of the most common axial and polar property tensors [26,29].

We are convinced that the presented results can serve as a useful reference for studies of the structure, domain phenomena, and tensor properties of ferroaxial materials, as well as for further development of the general theory of the macroscopic crystallographic symmetry lowering and its applications.

This work is supported by the Czech Science Foundation (Project No. 15-04121S).

*hlinka@fzu.cz

[1] R. D. Johnson, S. Nair, L. C. Chapon, A. Bombardi, C. Vecchini, D. Prabhakaran, A. T. Boothroyd, and P. G. Radaelli, $Cu_3Nb_2O_8$: A Multiferroic with Chiral Coupling to the Crystal Structure, Phys. Rev. Lett. **107**, 137205 (2011).

[2] R. D. Johnson, L. C. Chapon, D. D. Khalyavin, P. Manuel, P. G. Radaelli, and C. Martin, Giant Improper Ferroelectricity in the Ferroaxial Magnet $CaMn_7O_{12}$, Phys. Rev. Lett. **108**, 067201 (2012).

[3] N. Terada, D. D. Khalyavin, P. Manuel, W. Yi, H. S. Suzuki, N. Tsujii, Y. Imanaka, and A. A. Belik, Ferroelectricity induced by ferriaxial crystal rotation and spin helicity in a *B*-site-ordered double-perovskite multiferroic In_2NiMnO_6, Phys. Rev. B **91**, 104413 (2015).

[4] R. Yuan, L. Duan, X. Du, and Y. Li, Identification and mechanical control of ferroelastic domain structure in rhombohedral $CaMn_7O_{12}$, Phys. Rev. B **91**, 054102 (2015).

[5] H. Schmid, Some symmetry aspects of ferroics and single phase multiferroics, J. Phys. Condens. Matter **20**, 434201 (2008).

[6] I. I. Naumov, L. Bellaiche, and H. Fu, Unusual phase transitions in ferroelectric nanodisks and nanorods, Nature (London) **432**, 737 (2004).

[7] J. Hlinka, Eight Types of Symmetrically Distinct Vectorlike Physical Quantities, Phys. Rev. Lett. **113**, 165502 (2014).

[8] C. Ederer and N. A. Spaldin, Towards a microscopic theory of toroidal moments in bulk periodic crystals, Phys. Rev. B **76**, 214404 (2007).

[9] Yu. Sirotin and M. P. Shaskolskaya, *Fundamentals of Crystal Physics* (Mir, Moscow, 1982).

[10] K. Aizu, Possible species of ferroelectrics, Phys. Rev. **146**, 423 (1966).

[11] K. Aizu, Possible species of "ferroelastic" crystals and of simultaneously ferroelectric and ferroelastic crystals, J. Phys. Soc. Jpn. **27**, 387 (1969).

[12] K. Aizu, Possible species of ferromagnetic, ferroelectric, and ferroelastic crystals, Phys. Rev. B **2**, 754 (1970).

[13] Various flavors of the equivalence defining the species are discussed in, e.g., Refs. [14–16].

[14] K. Aizu, comprehensive tabulation of the four categories of ferroic point groups derived from each of the 31 prototype point groups, J. Phys. Soc. Jpn. **46**, 1716 (1979).

[15] V. Kopsky, Tensor parameters of ferroic phase transitions, Phase Transitions **73**, 1 (2001).

[16] D. B. Litvin, Tensorial classification of non-magnetic ferroic crystals, Acta Crystallogr. Sect. A **40**, 255 (1984).

[17] V. Janovec and J. Privratska, , in *International Tables for Crystallography, Volume D: Physical Properties of Crystals*, edited by A. Authier (Kluwer Academic, Dordrecht, 2003), Chap. 3.4.

[18] A. A. Tagantsev, L. E. Cross, and J. Fousek, *Domains in Ferroic Crystals and Thin Films* (Springer, New York, 2010).

[19] K. Aizu, Electrical, mechanical and electromechanical orders of state shifts in nonmagnetic ferroic crystals, J. Phys. Soc. Jpn. **32**, 1287 (1972).

[20] V. Janovec, M. Cmelik, and L. Machonsky, Piezoelectric and electrooptic ferroics–qualitative domain and tensor characteristics, Phase Transitions **83**, 670 (2010).

[21] J.-C. Toledano, V. Janovec, V. Kopsky, J. F. Scott, and P. Bocek, in *International Tables for Crystallography, Volume D: Physical Properties of Crystals*, edited by A. Authier (Kluwer Academic, Dordrecht, 2003), Chap. 3.1.

[22] V. Janovec, V. Dvorak, and J. Petzelt, Symmetry classification and properties of equi-translation structural phase transitions, Czech. J. Phys. B **25**, 1362 (1975).

[23] V. K. Wadhawan, *Introduction to Ferroic Materials* (Gordon and Breach, New York, 2000).

[24] J. F. Nye, *Physical Properties of Crystals* (Clarendon Press, Oxford, 1985).

[25] H. A. Jahn, Note on the Bhagavantam-Suranarayana method of enumerating the physical constants of crystals, Acta Crystallogr. **2**, 30 (1949).

[26] See Supplemental Material at http://link.aps.org/supplemental/10.1103/PhysRevLett.116.177602 for the (13×13)-sized property matrices of all 212 species.

[27] D. B. Litvin and V. Janovec, Spontaneous Tensor properties for multiferroic phases, Ferroelectrics **461**, 10 (2014).

[28] D. B. Litvin, Changes of physical properties in multiferroic phase transitions, Acta Crystallogr. Sect. A **70**, 382 (2014).

[29] Interactive lookup tool allowing one to access the (13×13)-sized property matrices of all 212 species is also available at http://palata.fzu.cz/species/13x13axial.

[30] Species numbers 36, 41, 51, 52, 73, 78, 107, 109, 114, 126, 127, and 132.

[31] Species numbers 36, 52, 73, 107, and 109.

[32] R. E. Newnham and L. E. Cross, Symmetry of secondary ferroics. I, Mater. Res. Bull. **9**, 927 (1974).

[33] R. E. Newnham and L. E. Cross, Symmetry of secondary ferroics. II, Mater. Res. Bull. **9**, 1021 (1974).
[34] A. T. Mulder, N. A. Benedek, J. M. Rondinelli, and C. J. Fennie, Turning ABO_3 Antiferroelectrics into ferroelectrics: Design rules for practical rotation-driven ferroelectricity in double perovskites and $A_3B_2O_7$ Ruddlesden-Popper compounds, Adv. Funct. Mater. **23**, 4810 (2013).
[35] E. Bousquet, M. Dawber, N. Stucki, C. Lichtensteiger, P. Hermet, S. Gariglio, J.-M. Triscone, and P. Ghosez, Improper ferroelectricity in perovskite oxide artificial superlattices, Nature (London) **452**, 732 (2008).
[36] N. A. Benedek and C. J. Fennie, Hybrid Improper Ferroelectricity: A Mechanism for Controllable Polarization-Magnetization Coupling, Phys. Rev. Lett. **106**, 107204 (2011).
[37] J. Valasek, Piezo-electric and allied phenomena in Rochelle salt, Phys. Rev. **17**, 475 (1921).
[38] T. Mitsui, Theory of the ferroelectric effect in Rochelle salt, Phys. Rev. **111**, 1259 (1958).
[39] T. Oja and P. A. Casabella, Nuclear-magnetic-resonance studies of ferroelectricity in normal and irradiated Rochelle salt, Phys. Rev. **177**, 830 (1969).
[40] Y. Akishige, G. Oomi, T. Yamamoto, and E. Sawaguchi, Dielectric properties of ferroelectric hexagonal $BaTiO_3$, J. Phys. Soc. Jpn. **58**, 930 (1989).
[41] A. Sawada, M. Udagawa, and T. Nakamura, Proper Ferroelastic Transition in Piezoelectric Lithium Ammonium Tartrate, Phys. Rev. Lett. **39**, 829 (1977).
[42] B. O. Hildmann, Th. Hahn, L. E. Cross, and R. E. Newnham, Lithium ammonium sulphate, a polar ferroelastic which is not simultaneously ferroelectric, Appl. Phys. Lett. **27**, 103 (1975).
[43] X. S. Xu, M. Angst, T. V. Brinzari, R. P. Hermann, J. L. Musfeldt, A. D. Christianson, D. Mandrus, B. C. Sales, S. McGill, J.-W. Kim, and Z. Islam, Charge Order, Dynamics, and Magnetostructural Transition in Multiferroic $LuFe_2O_4$, Phys. Rev. Lett. **101**, 227602 (2008).
[44] A. Glamazda, K.-Y. Choi, P. Lemmens, D. Wulferding, S. Park, and S.-W. Cheong, Charge gap and charge-phonon coupling in $LuFe_2O_4$, Phys. Rev. B **87**, 144416 (2013).
[45] N. Ikeda, T. Nagata, J. Kano, and S. Mori, Present status of the experimental aspect of RFe_2O_4 study, J. Phys. Condens. Matter **27**, 053201 (2015).
[46] J. D. Budai, J. Hong, M. E. Manley, E. D. Specht, C. W. Li, J. Z. Tischler, D. L. Abernathy, A. H. Said, B. M. Leu, L. A. Boatner, R. J. McQueeney, and O. Delaire, Metallization of vanadium dioxide driven by large phonon entropy, Nature (London) **515**, 535 (2014).
[47] A. Tselev, I. A. Luk'yanchuk, I. N. Ivanov, J. D. Budai, J. Z. Tischler, E. Strelcov, A. Kolmakov, and S. V. Kalinin, Symmetry relationship and strain-induced transitions between insulating M1 and M2 and metallic R phases of vanadium dioxide, Nano Lett. **10**, 4409 (2010).
[48] H.-H. Kung, R. E. Baumbach, E. D. Bauer, V. K. Thorsmolle, W.-L. Zhang, K. Haule, J. A. Mydosh, and G. Blumberg, Chirality density wave of the "hidden order" phase in URu_2Si_2, Science **347**, 1339 (2015).
[49] T. Yanagisawa, S. Mombetsu, H. Hidaka, H. Amitsuka, M. Akatsu, S. Yasin, S. Zherlitsyn, J. Wosnitza, K. Huang, and M. B. Maple, Γ_3-type lattice instability and the hidden order of URu_2Si_2, J. Phys. Soc. Jpn. **82**, 013601 (2013).